Two-dimensional magnetic switching of micron-size films in magnetic tunnel junctions

A. Anguelouch, B. D. Schrag, and Gang Xiao
Department of Physics, Brown University, Providence, Rhode Island 02912

Yu Lu, P. L. Trouilloud, R. A. Wanner, and W. J. Gallagher
IBM T. J. Watson Research Center, Yorktown Heights, New York 10598

S. S. P. Parkin
IBM Almaden Research Center, San Jose, California 95120

(Received 18 October 1999; accepted for publication 22 November 1999)

The magnetic switching behavior of micron-size magnetic tunnel junctions has been studied in two-dimensional magnetic fields. By measuring junction resistance, we obtain information about the magnetization state of the free ferromagnetic layer. Magnetic properties of this layer are explored using the Stoner–Wohlfarth rotational model as a starting point. We use geometric parameters of the critical curves to obtain information about interlayer coupling and domain structure effects in the free layer. © *2000 American Institute of Physics.* [S0003-6951(00)00304-1]

Magnetic tunneling junctions (MTJs) have been the subject of intense study since the discovery of large magnetoresistance (MR) in these devices at room temperature.[1,2] These devices have many properties which make them possible candidates for use in several technological applications, such as magnetic random access memory[3] (MRAM) devices. Because the memory cells in MRAM devices[3] require magnetic fields to be applied in two dimensions, it is important to study the response of tunneling junctions to fields applied along both the easy- and the hard-axis directions. In this letter, we present measurements of the properties of micron-size MTJs subject to two-dimensional magnetic fields in the plane of the device.

The MTJs studied in this experiment were grown via sputtering and patterned using electron-beam lithography, as described elsewhere.[4,5] A schematic of the sample is shown in Fig. 1(a). The layer sequence with thicknesses in angstroms is Si(100) substrate/50 Ta/250 Al/40 $Ni_{60}Fe_{40}$/100 FeMn/60 Co/7 Ru/30 Co/11 Al_2O_3/74 $Ni_{60}Fe_{40}$/250 Al/75 Ta. For this structure, the FeMn is the pinning layer, the Co/Ru/Co layer serves as the pinned electrode, and the 75 $Ni_{60}Fe_{40}$ layer serves as the free electrode. The thin layer of Ru between the two Co layers (P1 and P2) has the effect of antiferromagnetically biasing these two layers through interlayer exchange. Magnetic tunneling occurs between the free NiFe layer and the 30 Co (P1) layer, which are adjacent to the Al_2O_3 barrier on either side. Each patterned chip contains several hundred junctions of various shapes and sizes. In this letter, data on 11 different junctions are presented, all from the same chip. We studied rectangular samples with areas between 5 and 200 μm^2 and aspect ratios ranging from 3:1 to 16:1.

The MR of the MTJ samples was measured on a probe station equipped with a toroidal magnet which provides a two-dimensional field of up to 150 Oe. The magnetic field is relatively uniform ($\pm 2\%$ change) over the area of the sample, and the easy- and hard-axis fields were estimated to be perpendicular to within 2°. The voltage applied across the sample is on the order of several mV and the dc voltage bias is zero. The applied magnetic fields are low enough so that the pinned layer can be considered essentially fixed; hence, all of the data presented in this letter are assumed to be measurements of the properties of the free layer only.

In a typical measurement, the hard-axis field (H_y) was held at a fixed value while the easy-axis field (H_x) was swept linearly within ± 125 Oe, at a frequency of 10 Hz. For each sample, 500 MR loops were recorded, each containing 500 data points. A representative MR hysteresis loop is given in Fig. 1(b). For each sample, 40 fixed hard-axis fields

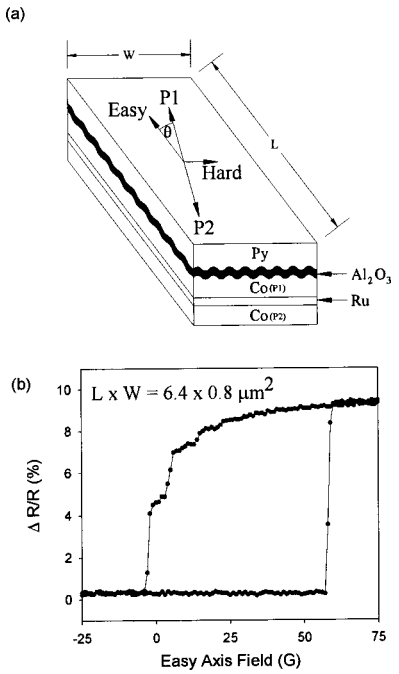

FIG. 1. (a) Schematic of the sample layer structure. The two cobalt layers will align antiparallel due to interlayer exchange across the thin Ru layer. Néel coupling occurs as a result of interface roughness at the tunneling barrier, as shown. The pinned axis (represented by P1 and P2) is assumed to be slightly misaligned with respect to the easy axis of the sample. (b) Mangetoresistance hysteresis loop, with zero applied hard-axis field.

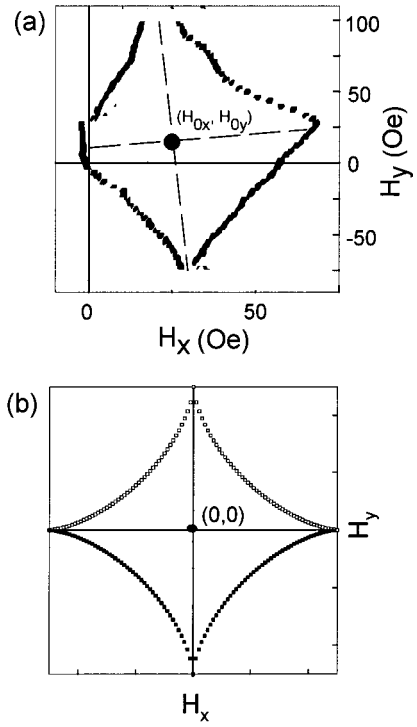

FIG. 2. (a) Asteroid curve of one representative MTJ with dimensions 0.8 $\times 6.4\ \mu m^2$. H_x and H_y are fields in the easy- and hard-axis directions. (b) Stoner–Wohlfarth critical curve for an ideal single-domain particle with uniaxial anisotropy.

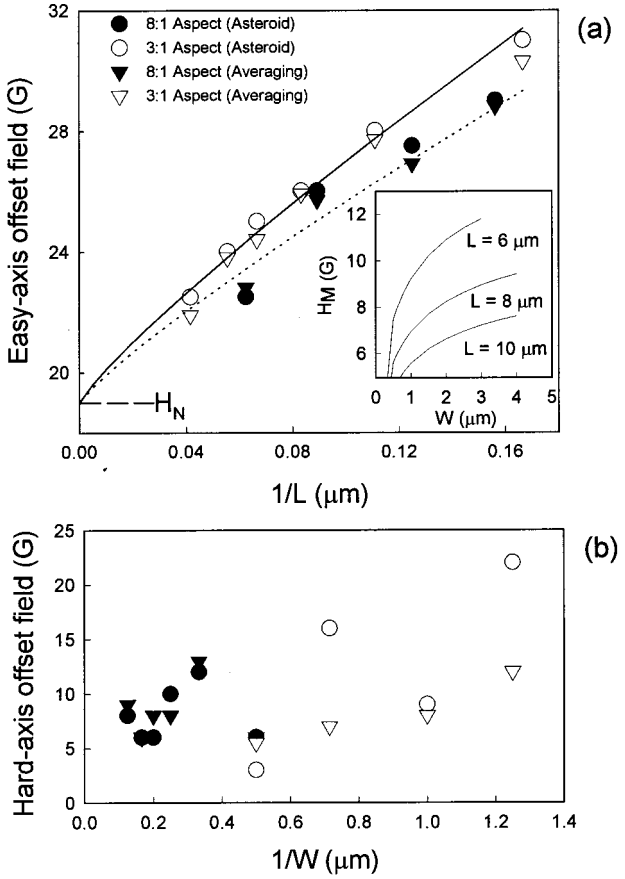

FIG. 3. (a) Easy-axis offset field as a function of $1/L$ and (b) hard-axis offset field as a function of $1/W$, where W and L are the sample width and length. Circles and triangles represent values obtained using the asteroid fitting and averaging methods, respectively. Solid (open) data points represent samples with 3:1 (8:1) aspect ratios. Lines are fits to the data for each aspect ratio, according to Eq. (2). The inset in (a) plots the theoretical magnetostatic coupling field obtained by computer simulations for three sample lengths as a function of sample width.

were selected, each separated by a few Oe. The switching field was defined as the magnetic field at which the resistance curve had maximum slope. We recorded two such points in field space (H_x, H_y) for each loop, one for the parallel to antiparallel magnetization switch and one for the reverse process. These points were plotted in two-dimensional (2D) field space to give the so-called ''asteroid'' curve[6,7] of each sample. Figure 2(a) shows one such curve.

For a single-domain particle with uniaxial anisotropy, the Stoner–Wohlfarth (SW) model[6] gives the shape of the critical asteroid curve, as shown in Fig. 2(b). It can be seen from Fig. 2 that the critical curves for our samples deviate significantly from the theoretical asteroid, while still retaining some of the expected features. This is to be expected from previous results,[8] which show that samples of this kind generally switch by complicated processes that can involve coherent rotation as well as domain-wall motion, and thus rarely exhibit SW single-domain behavior. The objective of our analysis is to characterize some of these deviations. In this work, we have measured five easily quantifiable parameters of each asteroid for comparison with theoretical values. The first two parameters were the coordinates of the center of the asteroid (H_{0x}, H_{0y}), as shown in Fig. 2(b). We also measured the dimensions of each asteroid along its natural axes, shown by dashed lines, and the angle at which these axes were tilted from the field axes.

Coordinates of the center of each asteroid in the H_x–H_y plane were measured by two different methods. In the first method, all of the data points in the asteroid were averaged to construct a mathematical mean offset in each field direction. The second method involved visually fitting the experimental data to theoretical SW curves by adjusting these five parameters. These data for H_{0x} and H_{0y} are plotted in Figs. 3(a) and 3(b) as functions of the inverse sample length and width, respectively. The SW model predicts an asteroid centered at the origin of field space. However, in MTJs there are many mechanisms which can shift hysteresis loops along the easy-axis direction.[9] The two important sources in our samples are Néel ''orange-peel'' coupling,[10] caused by interface roughness between the two magnetic layers [see Fig. 1(a)], and magnetostatic, or ''stray-field,'' coupling, caused by uncompensated magnetic poles at the edges of the bottom electrode.

The magnitude of the Néel coupling is given by[10]

$$H_N = \frac{\pi^2}{\sqrt{2}}\left(\frac{h^2}{\lambda t_F}\right) M_S \exp(-2\pi\sqrt{2}t_S/\lambda), \tag{1}$$

where h and λ are the amplitude and wavelength of the interface roughness, M_S is the saturation magnetization of the pinned layer, and t_F and t_S are the thicknesses of the free layer and spacer layer, respectively. All of these parameters are fixed for a given sample, therefore, we expect that the magnitude of the Néel coupling will be a constant for all of our samples. In contrast, stray-field coupling is dependent on

junction size and shape. It can be seen in Fig. 3(a) that there is a strong dependence of the easy-axis offset on sample length. Simulations we have done determined that for our sample geometry, the magnetostatic coupling field is given by

$$H_M = AW^{\alpha}/L, \tag{2}$$

where W and L are the sample width and length in microns, A is a constant, and $\alpha = 0.22$. The inverse relationship of stray-field coupling strength with sample length is expected from basic magnetostatic arguments, while the weak dependence on width is a result of the increased size of uncompensated poles in wider samples. The inset in Fig. 3(a) is a plot of the simulation results of H_M for samples with fixed length and changing width. It clearly shows that the width dependence of H_M is appreciable. The value of α is dependent on the sample dimensions; in the limit where the separation between the free layer and the relevant pinned layer is much larger than its width, the value of α should approach 1, whereas in the opposite limit, the value of α should be nearly zero. Therefore, we would expect the width dependence of the offset field to become more prominent (larger α) as the lateral dimensions of MTJs decrease.

The solid lines in Fig. 3(a) represent fits to the data incorporating a constant Néel coupling term in addition to the stray-field term above. It can be seen that this simple model agrees with the data quite well. The parameters of the fit, expressed in units of gauss and microns, are $A = 65$, $\alpha = 0.14$, and $H_N = 19$ G. The theoretical and experimental magnitudes, represented by the constant A, agree to within 10%. In addition, the Néel coupling field of the bulk sample was independently measured to be 20 G, in good agreement with the fitted value. The small discrepancy between experimental and simulated values of α could be caused by micromagnetic factors not addressed by our simple simulation.

Figure 3(b) gives values for the hard-axis field offset H_{0y} of our samples as a function of sample width. These values have much higher errors than those quoted in Fig. 3(a) because the deformation of the asteroid is greatest along the easy axis. However, it appears that the width dependence of the offset field is similar to that described above. We postulate that this effect arises as a result of an angular mismatch between the pinned layer magnetization direction and the easy axis, which would give rise to Néel and stray-field coupling components along the hard axis. Assuming this mismatch θ [see Fig. 1(a)] is small, the magnitude of each of these effects can be related to the magnitude of the easy-axis offset field according to

$$H_{0Y} = H_{0X} \tan\theta = (H_N + AL^{\alpha}/W)\tan\theta, \tag{3}$$

where we have interchanged L and W because the stray-field coupling is now perpendicular to the easy axis. From rough fits to Fig. 3(b), it appears the Néel coupling strength is approximately 2 G and the stray-field coupling constant $A \tan\theta$ is roughly equal to 11 G. Dividing these magnitudes by the fitted values for H_N and A for the easy-axis case gives estimated values of the mismatch angle θ ranging from 5° to 10°. We believe that this small mismatch may have resulted from misalignment during sample annealing.

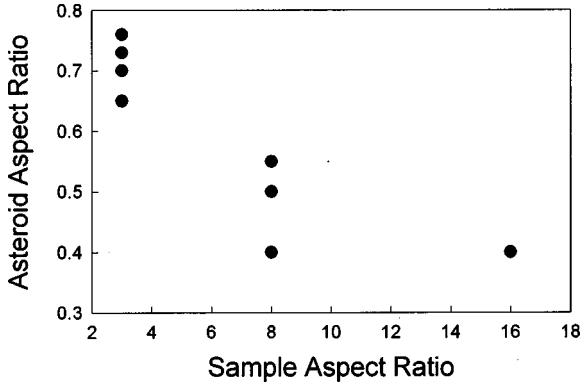

FIG. 4. Ratio of easy-axis to hard-axis dimension of each asteroid as a function of sample aspect ratio.

We now address the issue of asteroid shape in relation to geometrical parameters of micron-size films. The asteroid shape is sensitive to domain formation and switching modes. For single-domain particles, the SW switching curve is symmetrical with a unit asteroid aspect ratio, defined as the ratio of the maximum length of the asteroid curve along the easy axis to that along the hard axis. All of our samples yield an elongated asteroid along the hard axis. Figure 4 shows that the asteroid aspect ratio decreases with increasing geometrical aspect ratio of the rectangular films. Lu *et al.* have proposed[11] that the reduced asteroid aspect ratio is due to the existence of edge domains. Because it is energetically favorable to have spins aligned along the edges of a sample, these edge domains will lag the bulk of the sample in aligning themselves with the external filed. For a more needle-like sample, a larger portion of spins is confined in the edge domains. It would require a larger hard axis-field to align these spins near the edges; hence, a smaller asteroid aspect ratio. Our data in Fig. 4 are consistent with this explanation.

This work was supported by National Science Foundation Grant No. DMR-9701579, and partially by Defense Advanced Research Projects Agency Contract Nos. MDA972-96-C-0030 and MDA972-99-C-0009.

[1] J. S. Moodera, L. R. Kinder, T. M. Wong, and R. Meservey, Phys. Rev. Lett. **74**, 3273 (1995).
[2] N. Tezuka and T. Miyazaki, J. Magn. Magn. Mater. **139**, L231 (1995).
[3] S. S. P. Parkin, K, P. Roche, M. G. Samant, P. M. Rice, R. B. Beyers, R. E. Scheuerlein, E. J. O'Sullivan, S. L. Brown, J. Bucchigano, D. W. Abraham, Y. Lu, M. Rooks, P. L. Trouilloud, R. A. Wanner and W. J. Gallagher, J. Appl. Phys. **85**, 5828 (1999).
[4] S. A. Rishton, Y. Lu, R. A. Altman, A. C. Marley, X. P. Bian, C. Jahnes, R. Viswanathan, G. Xiao, W. J. Gallagher, and S. S. P. Parkin, Microelectron. Eng. **35**, 249 (1997).
[5] W. J. Gallagher, S. S. P. Parkin, Y. Lu, X. P. Bian, A. Marley, K. P. Roche, R. A. Altman, S. A. Rishton, C. Jahnes, T. M. Shaw, and G. Xiao, J. Appl. Phys. **81**, 3741 (1997).
[6] E. C. Stoner and E. P. Wohlfarth, Philos. Trans. R. Soc. London, Ser. A **240**, 599 (1948).
[7] J. C. Slonczewski, Research Memo No. 003.111.224, IBM Research Center, Poughkeepsie, NY (1956) (unpublished).
[8] S. Middlehoek, IBM J. Res. Dev. **4**, 394 (1962); M. Labrune, J. C. S. Kools, and A. Thiaville, J. Magn. Magn. Mater. **171**, 1 (1997).
[9] K.-S. Moon, R. E. Fontana, Jr., and S. S. P. Parkin, Appl. Phys. Lett. **74**, 3690 (1999).
[10] L. Néel, Comptes Rendus Acad. Sci. **255**, 1676 (1962).
[11] Y. Lu, P. L. Trouilloud, D. W. Abraham, R. Koch, J. Slonczewski, S. Brown, J. Bucchignano, E. O'Sullivan, R. A. Wanner, W. J. Gallagher, and S. S. P. Parkin, J. Appl. Phys. **85**, 5267 (1999).